Laser-Launched Flyer Experiments on Nickel – Titanium Alloy

Damian C. Swift*and Robert Hackenberg
P-24 Plasma Physics MST-6 Materials Science
MS E-526 MS G-755
Los Alamos National Laboratory †
Los Alamos, NM 87545, USA

LA-UR-02-1658 – March 19, 2002

Abstract

Shock waves were induced in samples of nickel – titanium alloys by the impact of laser-launched flyers. The flyer was either copper, or the same alloy as the target. Point and line VISAR systems were used to measure the acceleration of the flyer and the surface velocity history of the target. Flyer velocities ranged from ∼150 to 600 m/s, for a flyer ∼4 mm in diameter. Targets were between ∼100 and 400 μm thick. The target was either free or in contact with a PMMA window. The velocity histories were used to deduce points in the equation of state, and the flow stress. Flyers and targets were recovered from all experiments with a window.

Contents

*dswift@lanl.gov
†This work was performed under the auspices of the U.S. Department of Energy under contract # W-7405-ENG-36.

Table 1: Alloy compositions.

alloy	**composition** (atomic % Ni)
5B	52.5
6B	55.6

1 Introduction

This work was performed in support of the LDRD-ER starting in FY 2000 on the dynamics of martensitic phase changes, using nickel – titanium (NiTi) alloys as the prototype. We previously used the TRIDENT laser to induce shock waves in NiTi samples by direct illumination; a decaying shock wave was produced in these experiments [1, 2]. The recovered samples were sectioned and metallographical analysis was performed to investigate the effect of the shock loading on the microstructure [4]. Quantum mechanical calculations were made to predict the cold compression curve of NiTi [3], and a Grüneisen equation of state (EOS) was constructed from these calculations [5], in order to allow the loading history to be estimated at different positions within the samples. The experiments described here were intended to help validate this theoretical EOS, by using the better-characterised shock states generated by flyer impact. In many cases the samples were recovered after the experiments, so metallographical analysis could be performed in future if desired.

To generate shock states by impact, the TRIDENT laser was used to launch copper and NiTi flyers, each of which then impacted a stationary target comprising NiTi and transparent windows. The flyer speed and surface velocity of the sample were measured by Doppler velocimetry.

The laser pulse was ~600 ns long, and the flyers were ~50 to 200 μm thick. Velocities were a few hundred meters per second with a laser energy of ~5 to 20 J over a spot ~4 mm in diameter.

The experiments reported here were performed at TRIDENT between 18 and 20 December 2001.

2 Sample preparation

Ingots of Ni-Ti binary alloys were prepared from high-purity elements by arc melting and then arc-casting into cylinders. The composition of each ingot was chosen by controlling the relative amount of each element (Table. 1). The ingots were homogenized at 1100^{o}C for 50 hours and water quenched. Disc specimens of 5 mm diameter were cut from the ingots and ground and polished down to the desired thickness for the flyer plate shots. Complete discs were used as flyer plates while half discs were used as targets. The sample thickness was determined by making micrometer measurements at different points on each sample, in particular the center and edges.

3 Flyer impact experiments

Several different types of flyer experiment were performed. In all cases, the sample was semicircular, so the flyer could be seen and its velocity measured.

In some experiments, the sample was attached to a plane circular window made of PMMA (Fig. 1). The window allowed the sample and flyer to be recovered without subjecting them to unknown loads. The surface velocity of the sample is affected by the presence of a window, but the EOS of PMMA is known, so the shock state can still be deduced. The impact of the flyer with the window provides a reference time, allowing the shock transit time through the sample to be estimated, if the flyer speed can be measured with sufficient accuracy.

An inherently more accurate scheme was used in other experiments, where the PMMA window was split into two halves, and assembled so that the surface of one half of the window was flush with the impact face of the sample (Fig. 2). The impact of the flyer with this half of the window provided a time fiducial for the start of the shock wave in the sample, to the accuracy with which the surfaces could be make co-planar.

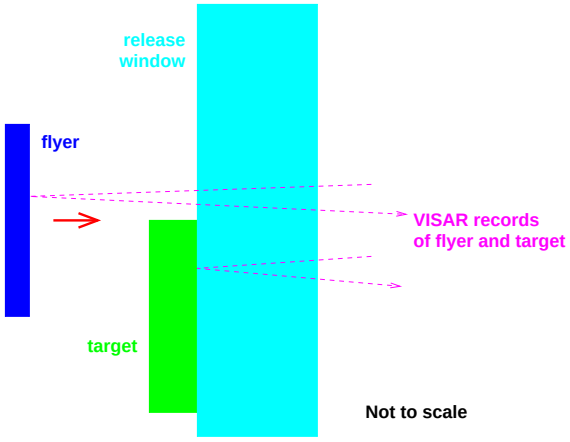

Figure 1: Schematic of experiments with a circular window.

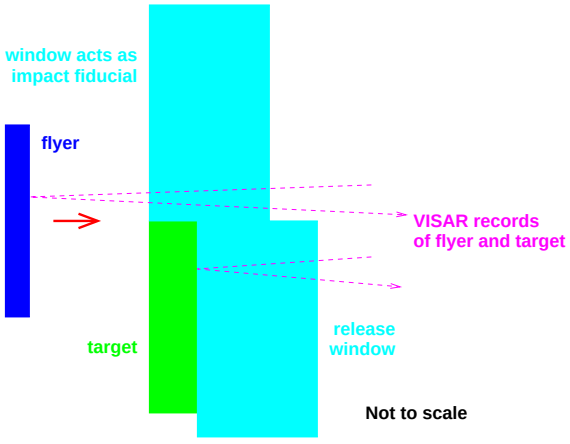

Figure 2: Schematic of experiments with an impact fiducial window and a release window.

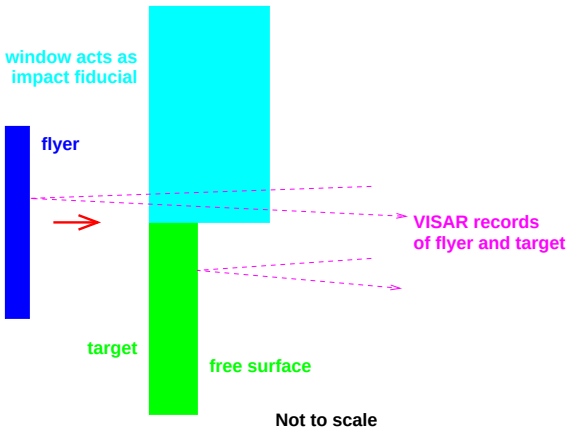

Figure 3: Schematic of experiments with an impact fiducial and no release window.

A modified design was used when problems were experienced with reflections from the window interfering with the signal from the sample. The window covering the sample was omitted, so the free surface velocity of the sample was measured rather than the interface velocity with PMMA (Fig. 3). It was not possible to recover samples from this type of experiment.

In experiments with a NiTi flyer, the impact of the flyer with the window also provides an EOS point, though with no information on the contribution from strength.

3.1 Target assembly

PMMA substrates were used, coated with ∼micron layers of carbon, aluminium, and alumina, in order to absorb the laser energy and insulate the flyer from heating [6].

Copper foils were purchased from Goodfellow Corp; most flyers were punched from this stock. The foils had distinct striations and machining marks. We attempted to remove these from the surface to avoid the generation of interference patterns which might interfere with the laser velocimetry measurements, by polishing the surface manually using diamond paste. This was only partially successful.

Each flyer was attached to its substrate with five-minute epoxy, the flyer being pressed down to minimize the thickness of the glue layer. In the limited time available, we did not measure the thickness of the glue bond.

For targets with a release window, the sample was positioned with a straight edge along a diameter of the disc, in the centre of the window. A small amount of five-minute epoxy was dropped on each corner of the sample.

For step-disc targets, the step-disc was constructed before adding the sample, The step height was fixed by resting one half-disc on the sample (and an additional sample of the closest match in thickness, for stability). Drops of five-minute epoxy were used to bond the step together. When set, the sample was positioned against the centre of the step, and epoxy was dropped at the corners of the sample. Sections of the spacer ring material were used along the circumference of the assembly, so that it presented a constant axial extent when assembled.

For impact fiducial targets, the sample and the window were positioned together on a flat surface, and five-minute epoxy dropped at the two corners of the sample in contact with the window.

In these experiments, PTFE tape was attached to the lab bench to provide a non-stick surface for target assembly. The tape had small-scale wrinkles, which probably contributed to misalignment where surfaces were intended to be co-planar.

The complete assembly was screwed together in a target holder.

3.2 Diagnostics

We used the Johnson line VISAR and a point VISAR to measure the velocity history of the flyer. The input/output optics were as described previously [6].

Lenses were used to image the target through the VISAR (i.e. focused at infinity) to the slit of the streak camera. Timing markers were incorporated on the streak record, at intervals of 200 ns. As before, the probe laser was made to produce a long ($\sim$1.5 μs) pulse to be able to capture the acceleration and impact of the flyer. The fringe constant of the VISAR was computed [8] from the thickness of the delay element (9.970" of BK7 glass). The dispersion of the glass was determined at the wavelength of the probe laser by fitting a straight line to points sampling the variation of refractive index with wavelength [9]. The fringe constant deduced was 216 m/s for a probe wavelength of 660 nm.

Relative timing of the point and line VISARs was deduced by comparing the position at which a shock wave appeared in a flyer impact experiment (shot 14123). The relative timing had an uncertainty of $\sim$3 ns.

3.3 Drive beam

TRIDENT was operated in long-pulse mode, as in the previous flyer work [6]. The drive pulse was chosen to be $\sim$600 ns long (full width, half maximum). The pulses generated were asymmetric in time, with a long tail.

An IR random-phase plate (RPP) was added to smooth the beam; this made a significant difference to the spatial uniformity. The beam optics were arranged to give a spot $\sim$4 mm in diameter on the substrate. The drive energy was quite low, so no RPP shield was included. The RPP collected a small amount of debris from the substrate, but was not significantly damaged. The surface of the RPP became misty after a couple of shots; this did not degrade the energy imparted to the flyer to any appreciable extent, and no larger-scale damage was observed after repeated firings through the same region of the RPP (as was feared if the misty layer absorbed much of the laser energy). We moved the RPP to expose a fresh region once during this series of experiments. The cause of the misting was not determined; one possibility was thought to be the oxidation of a layer of grease collected during storage. However, a surface previously cleaned with ethanol also became misty.

3.4 Flyer acceleration time and distance

The velocity history was measured initially for copper flyers [7], over the range of areal mass and laser energy planned for the NiTi experiments. The distance – time relation was obtained by numerical integration of the velocity history. The records generally indicated an appreciable acceleration at quite late times (corresponding to a residual pressure of a few tens of MPa). A point was chosen at which the acceleration had fallen to a reasonably low level; this was used to choose a 'barrel' space between the flyer and target, and to estimate the impact time and hence to choose time frames for the VISARs. The acceleration time was generally close to 1 μs.

4 Results

Fourteen NiTi experiments were performed, eleven with composition 5B and three with 6B (Table 2).

The drive energy was measured with a calorimeter, and the irradiance history of the drive pulse with a photodiode. The uncertainty in energy was of the order of 1 J. The pulse shape was reasonably repeatable at the same and different energies.

The VISAR records were used to measure the velocity history and flatness of each flyer. In some experiments, we recorded the impact of the flyer with a window and thus were able to measure the flatness directly after several hundred microns of flight. Most of the flyers were still accelerating slightly at the end of the record. There was evidence of ringing during acceleration, but no sign of shock formation or spall in the flyers.

The flatness of each flyer was measured with the line-imaging VISAR. Apart from a slight lag at the edges, all the flyers were flat to within the accuracy of the data. In most cases, the accuracy was dominated by the uncertainty in spatial wavelength of the fringes.

Table 2: NiTi flyer experiments.

Shot	Flyer			Target		Design	Comments
	material	thickness (μm)	speed (m/s)	material	thickness (μm)		
14123	NiTi 5B	90	440 ± 20	NiTi 5B	191	release window	
14124	NiTi 5B	102	430 ± 20	NiTi 5B	197	release window	
14125	NiTi 5B	108	200 ± 10	NiTi 5B	202	release window	
14141	NiTi 5B	201	240 ± 10	NiTi 5B	403	step-disc	
14142	NiTi 5B	207	280 ± 10	NiTi 5B	404	step-disc	
14143	NiTi 5B	209	230 ± 5	NiTi 5B	409	step-disc	
14144	NiTi 5B	154	275 ± 5	NiTi 5B	300	impact fiducial	
14146	NiTi 5B	156	365 ± 5	NiTi 5B	305	impact fiducial	
14147	Cu	55	324 ± 1	NiTi 5B	88	impact fiducial	
14148	Cu	55	573 ± 2	NiTi 5B	91	impact fiducial	fringes not clear
14149	Cu	55	556 ± 2	NiTi 5B	95	impact fiducial	
14150	Cu	55	615 ± 3	NiTi 6B	113	impact fiducial	
14151	NiTi 6B	90	335 ± 2	NiTi 6B	211	impact fiducial	
14152	NiTi 6B	222	147 ± 3	NiTi 6B	414	impact fiducial	

Table 3: Results from release window experiments.

shot	peak interface speed (m/s)	duration (ns)
14123	395 ± 5	6 ± 1
14124	390 ± 10	5 ± 2
14125	190 ± 5	42 ± 2

4.1 Release window

The release window design (Figs 1, 4 and 5) was used in the first three shots (14123 to 14125), because the semicircular PMMA windows required for the other types of experiment had not been delivered by then. The point VISAR was used to look at the surface of the sample.

Reflections from the window obscured the signal, so problems were encountered in interpreting the fringe motion. After impact with the sample, there was evidence of a surface wave moving across the flyer from the edge of the impact point, and a slower-moving jet. The impact of the flyer with the window was not recorded with adequate time resolution for the shock speed in the sample to be deduced, and the deceleration of the flyer on impact was also difficult to determine from the line VISAR records against the background of the window reflection. The fringe motion at the target – window interface was observed with reasonable clarity, allowing velocities to be deduced (Table 3). The line VISAR signal indicated that the flyer impact was acceptably flat. A precursor reached the surface of the sample ahead of the main shock. (Figs 6 to 8.)

4.2 Step-disc

The next three experiments (14141 to 14143) used the step-disc design (Figs 2, 9 and 10). Again, the signal from the flyer was obscured by reflections from the window. The point VISAR, less affected than the line VISAR by window reflections, was used to measure the flyer acceleration and impact with the fiducial window. (Table 4). The line VISAR record showed some spatial variation in arrival time. This was probably caused partly by misalignment of the sample with the surface of the fiducial window, and partly by the target assembly being tilted in the sample holder. The tilt was not great enough to compromise the accuracy of

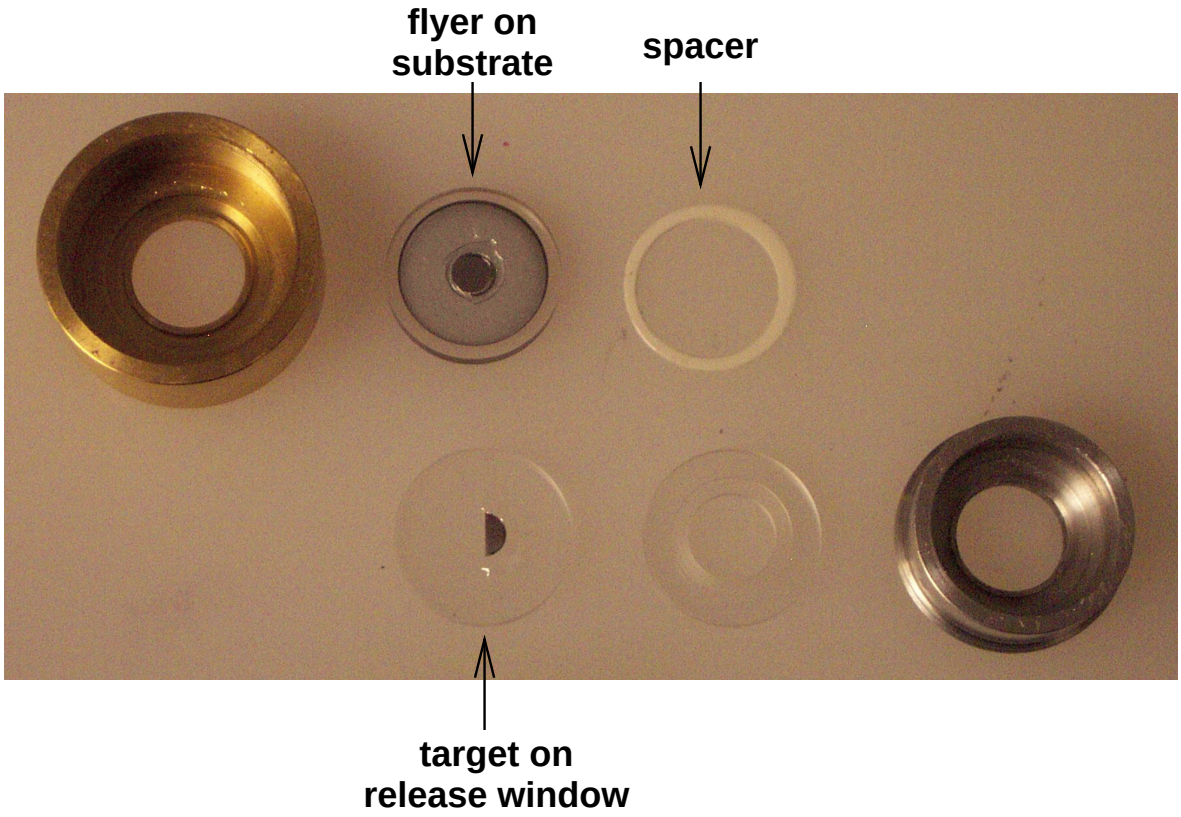

Figure 4: Release window components before final assembly (shot 14124).

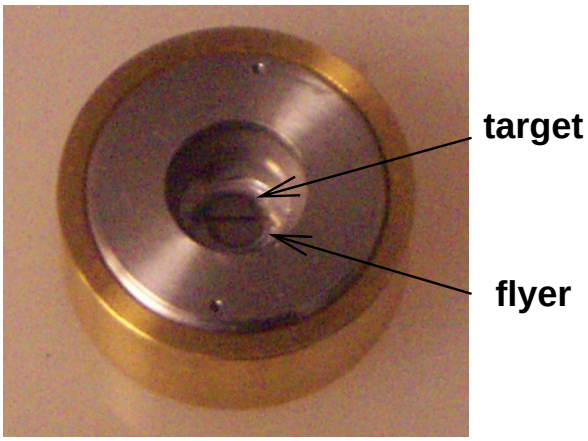

Figure 5: Release window components after final assembly (shot 14124).

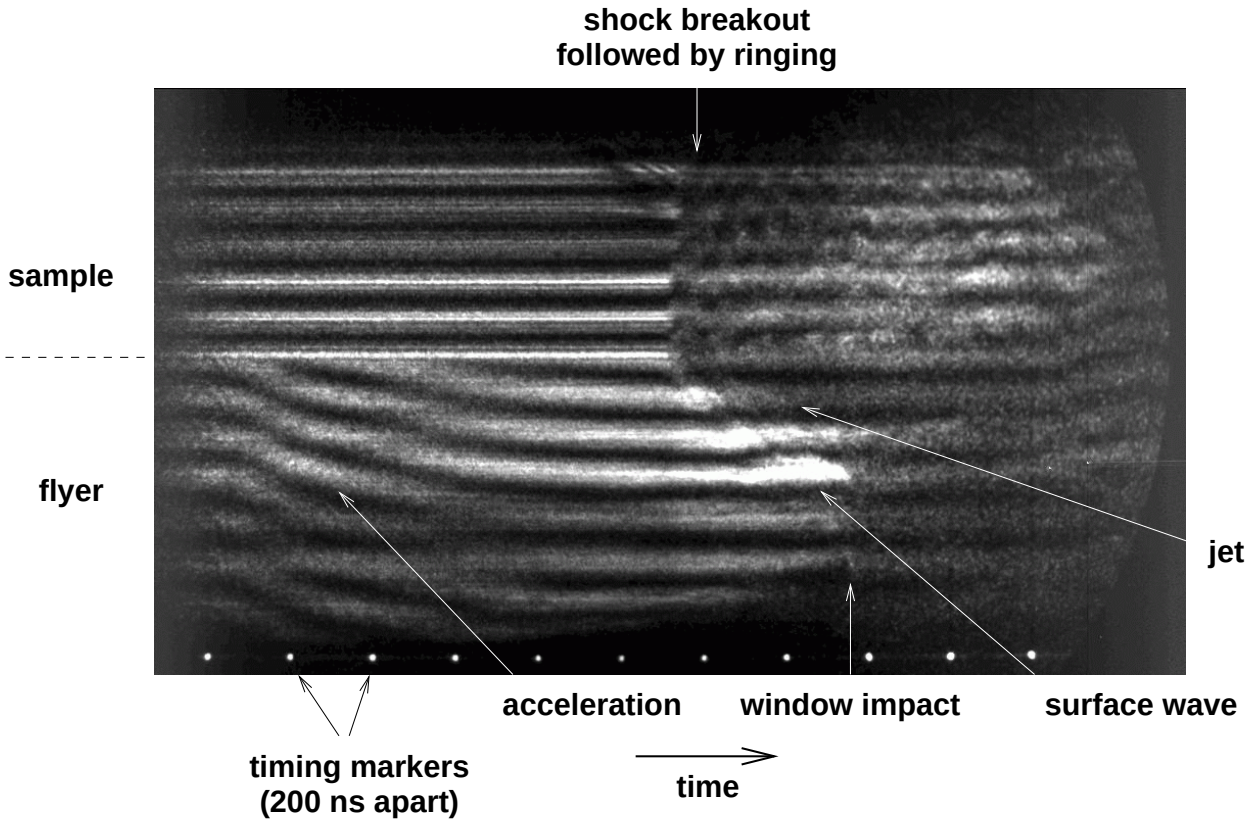

Figure 6: Example of line VISAR record from a window release experiment (shot 14124).

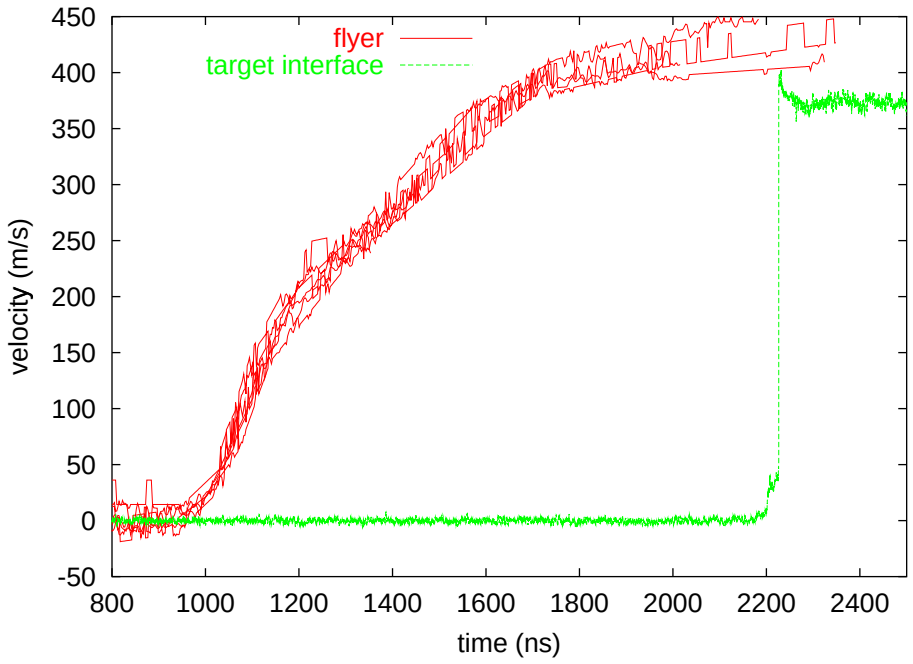

Figure 7: Example of velocity history for flyer and sample surface from a window release experiment (shot 14123).

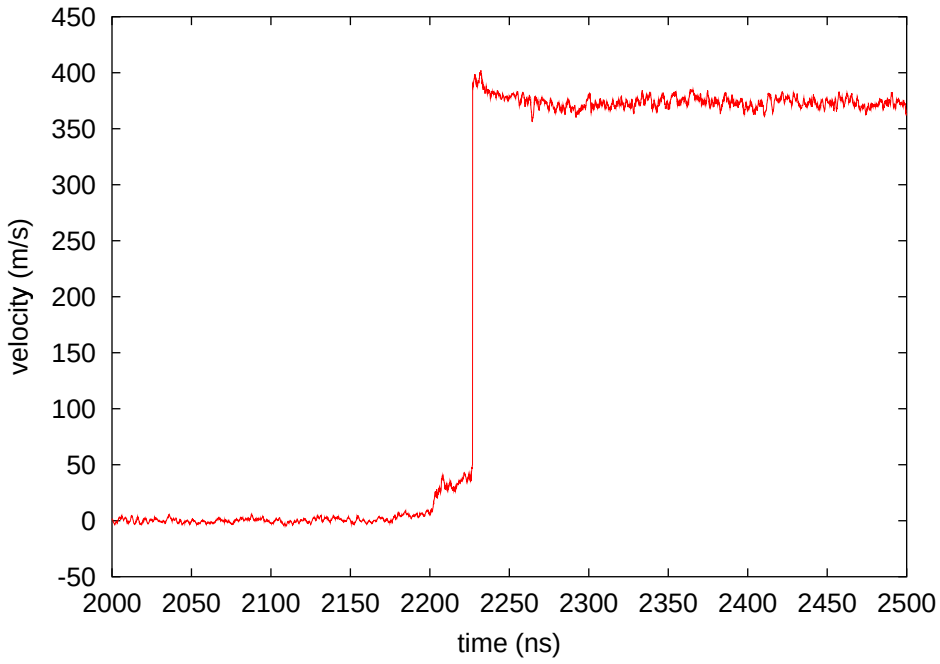

Figure 8: Example detail of precursor and main shock at sample surface from a window release experiment (shot 14123).

Table 4: Results from step-disc experiments.

shot	**fiducial speed** (m/s)	**precursor speed** (m/s)	**precursor delay** (ns)	**peak speed** (m/s)	**peak delay** (ns)
14141	110 ± 10	70 ± 10	130 ± 10	220 ± 20	190 ± 10
14142	120 ± 5	50 ± 10	20 ± 10	200 ± 20	30 ± 10
14143	110 ± 10	–	–	230 ± 10	–

the experiment.

The number of shots was limited, so it was not possible to perform repeated experiments to refine the time resolution of the streak camera. In addition, the flyer speed was low compared with the shock speed, so mis-alignments between the impact window and the sample caused a relatively large uncertainty in arrival time. (In this series of experiments, there was no opportunity to measure any misalignment and hence make a correction.) For these reasons, it was not possible to obtain an accurate shock transit time through the sample.

4.3 Impact fiducial

The remainder of the experiments used the impact fiducial design, allowing the NiTi sample to release into vacuum (Figs 3, 11 and 12).

The point VISAR was positioned to observe the flyer acceleration and deceleration following impact with the window (Table 5).

In the line VISAR records, the fringe contrast was poor in shot 14148 and the streak period began too late in shot 14150. No useful data were obtained from either record. Again, reflections from the window obscured the signal from the flyer. The copper flyers were more reflective than the NiTi, so a reasonable signal was obtained in these cases. Looking at the free surface of the sample, if was generally possible to

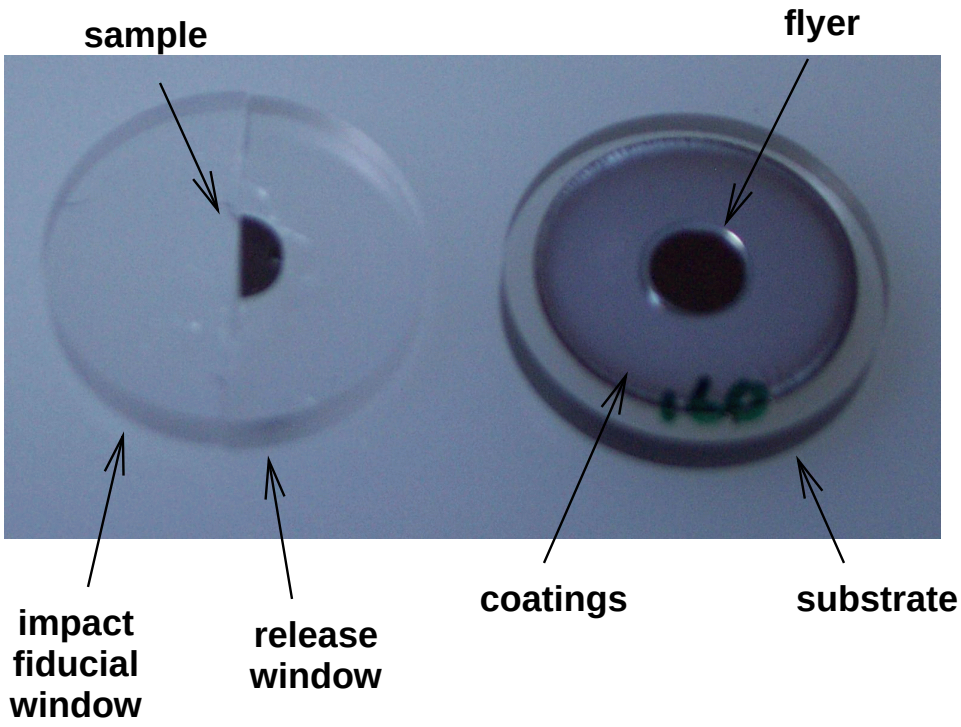

Figure 9: Step-disc components before final assembly (shot 14143).

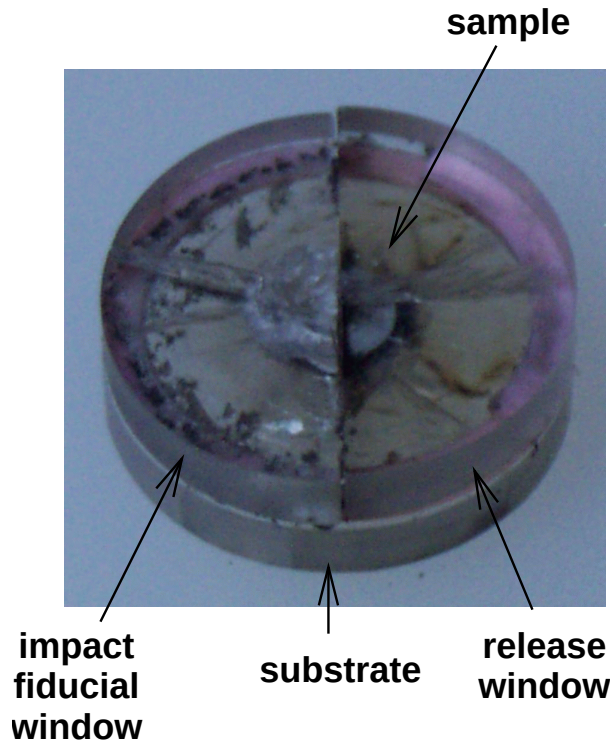

Figure 10: Step-disc components after recovery (shot 14143).

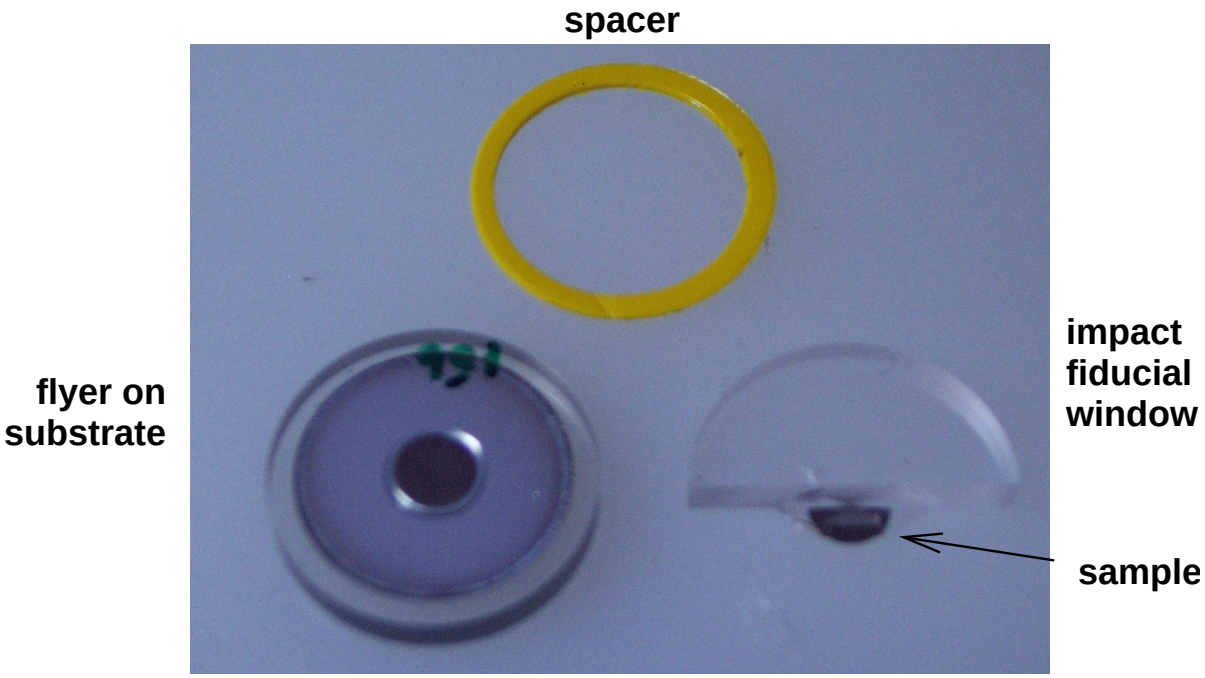

Figure 11: Fiducial window components before final assembly.

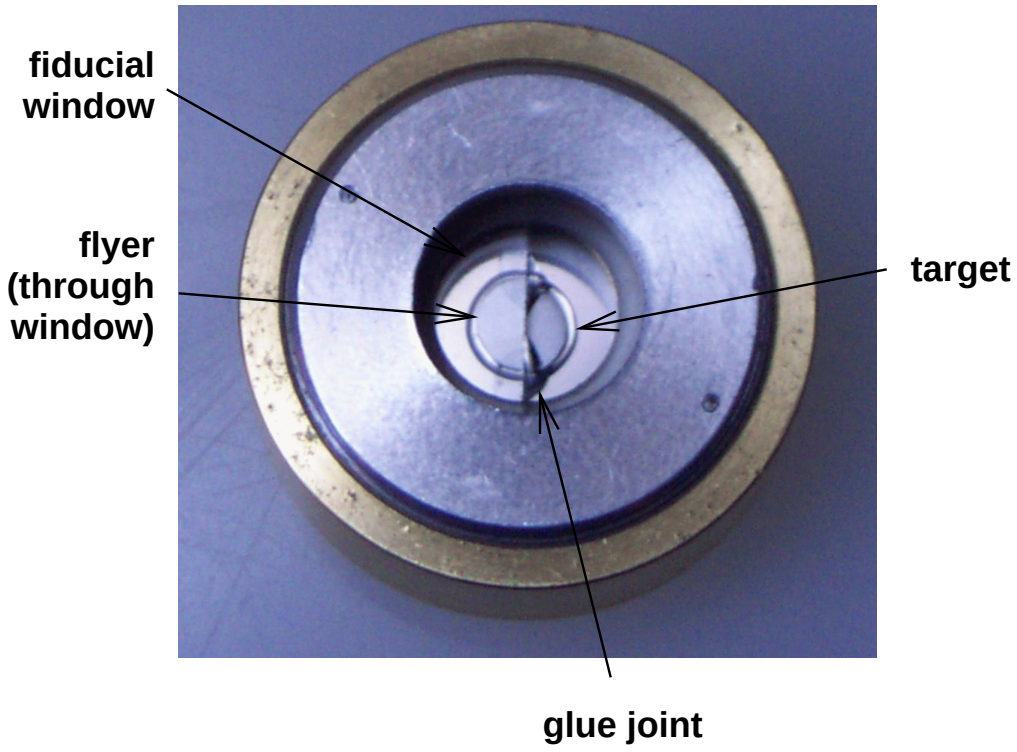

Figure 12: Fiducial window components after final assembly.

Table 5: Point VISAR deceleration results from impact fiducial experiments.

shot	**post-impact speed** (m/s)
14144	259 ± 3
14146	321 ± 3
14147	295 ± 5
14148	521 ± 3
14149	503 ± 2
14151	292 ± 2
14152	130 ± 2

Table 6: Line VISAR results from impact fiducial experiments.

shot	**release speed** (m/s)	**pull-back** (m/s)
14146	–	120 ± 20
14147	375 ± 25	100 ± 25
14149	520 ± 50	110 ± 20
14150	720 ± 50	130 ± 10
14151	300 ± 20	180 ± 30

see the peak free surface velocity and also the pull-back in velocity as the rarefaction from the rear surface of the flyer passed through the sample (Table 6). The line VISAR record showed some spatial variation in the arrival time of the shock at the surface of the sample. The samples in these experiments were attached to the window at only two points, so the spatial variation was probably caused mainly by the sample tilting with respect to the window if assembled before the epoxy was completely set. The spatial variation in some experiments was caused partly by the target assembly being tilted in the sample holder – since only a half-disc of window was used, there was a greater chance of tilt. This could be seen as a spatial variation in the signal from the window side of the line VISAR record. The tilt was not great enough to compromise the accuracy of the experiment. (Figs 13, 14, and 15.)

5 Equation of state and strength

The reduced data were used to infer EOS and strength properties.

5.1 Method of analysis

The impact of a NiTi flyer with the window provided a direct measurement of a point on the principal Hugoniot, with reference to the principal Hugoniot for the window (Fig, 16).

The impact of a NiTi flyer onto a NiTi target, releasing into a window, allowed a point on the principal Hugoniot to be deduced approximately, relying on the assumption that the NiTi release isentrope through the shock state generated by the impact was equal to the principal Hugoniot (Fig. 17). At the pressures of a few GPa generated in these experiments, this assumption is likely to be reasonably accurate.

Similarly, the release analysis could be applied when the flyer was a material of known properties (Fig. 18). The simplest case is for release into vacuum, where the particle speed in the sample can be estimated as half of the free surface speed. The difference between this and the flyer speed is equal to the particle speed in the flyer, and the Hugoniot of the flyer material can be used to find the shock pressure.

Where the shock speed could be deduced, this allowed a direct measurement of a point on the Hugoniot in shock speed – particle speed coordinates, the particle speed in the shocked state being half of the flyer

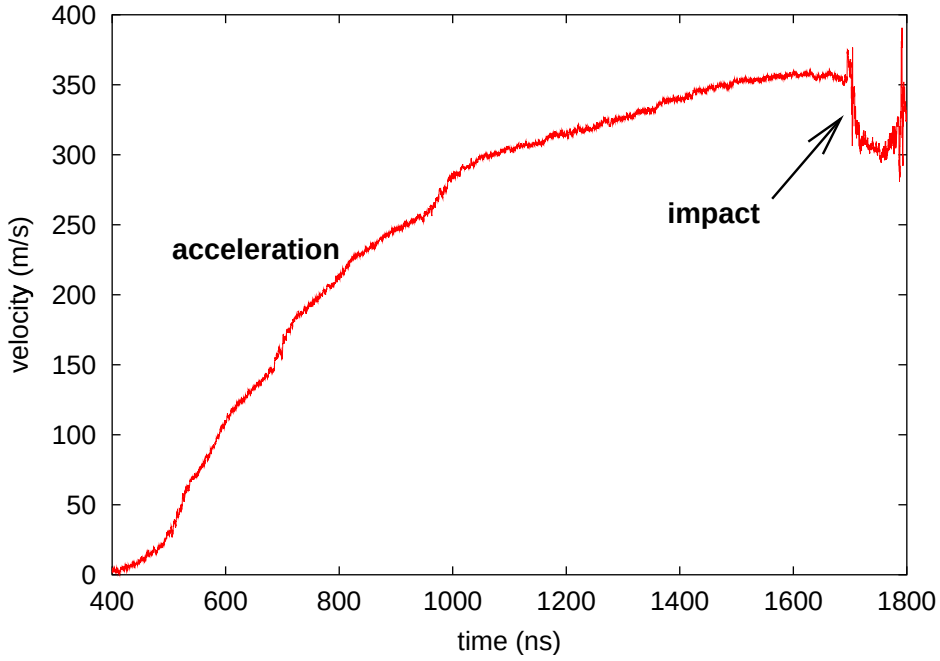

Figure 13: Example flyer acceleration followed by window impact from fiducial window experiment (shot 14146; point VISAR record).

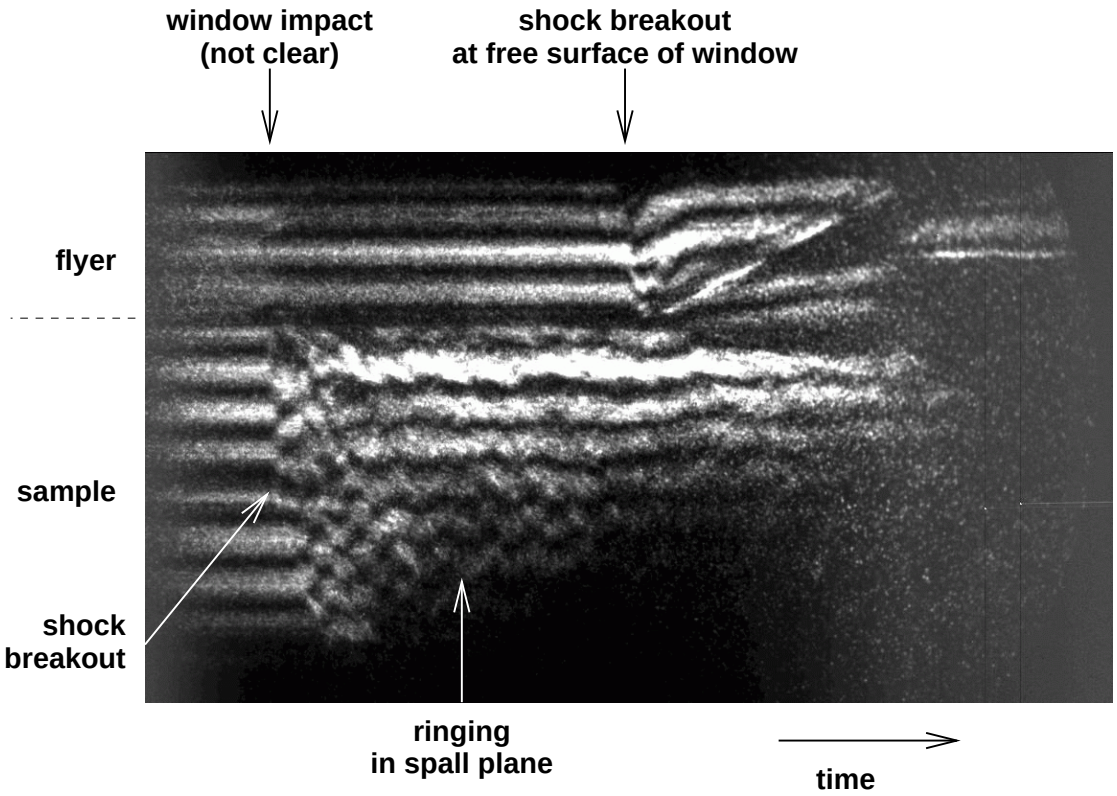

Figure 14: Example line VISAR record from fiducial window experiment (shot 14146).

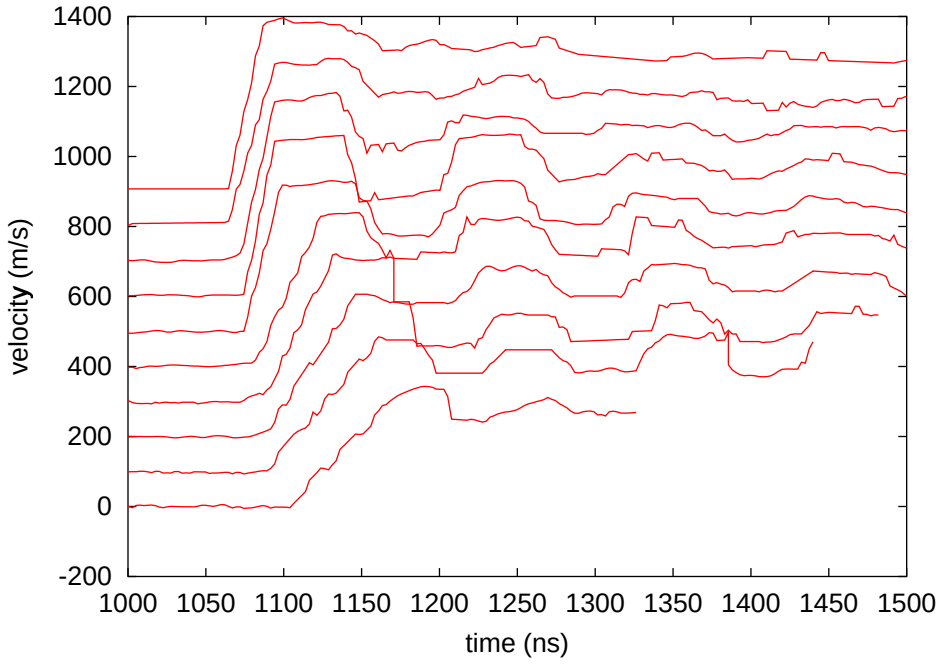

Figure 15: Example velocity history at free surface of sample from fiducial window experiment (shot 14146; line VISAR record; record from adjacent fringes displaced by 100 m/s for clarity).
The rising part of the shock wave appears wider at the edge – where the shock arrival was delayed in time – because the velocity history from each fringe moves across the surface of the sample. Considering a fixed point on the surface, the shock wave had an instantaneous rise at all locations.

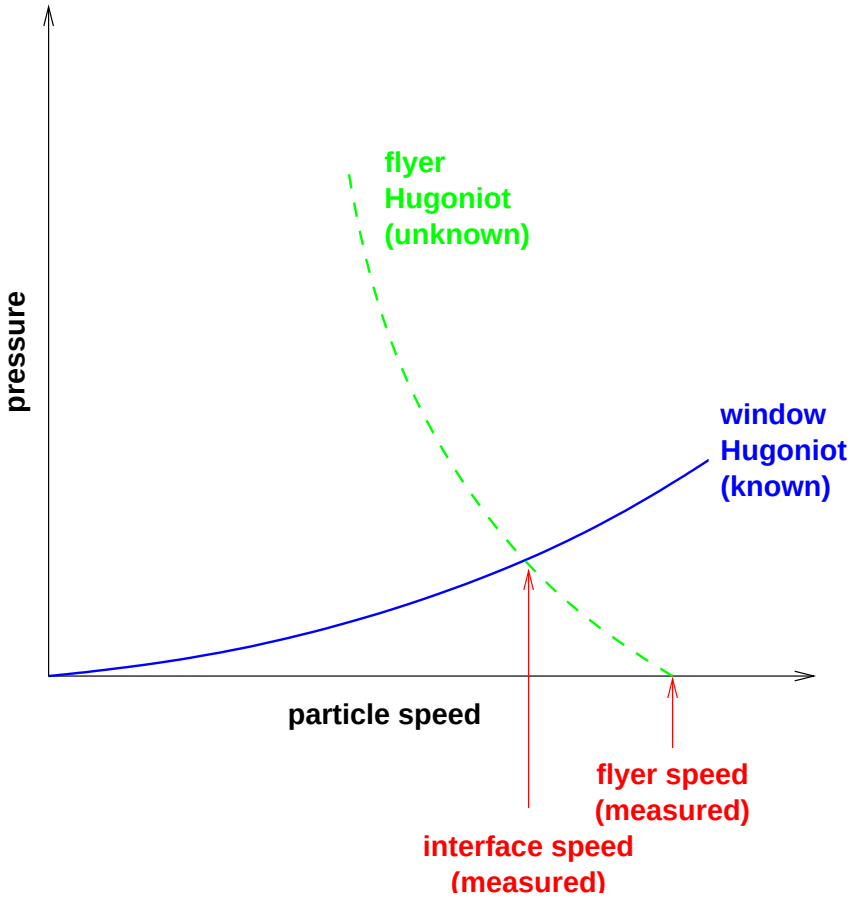

Figure 16: Schematic of construction used to deduce Hugoniot point from window impact data.

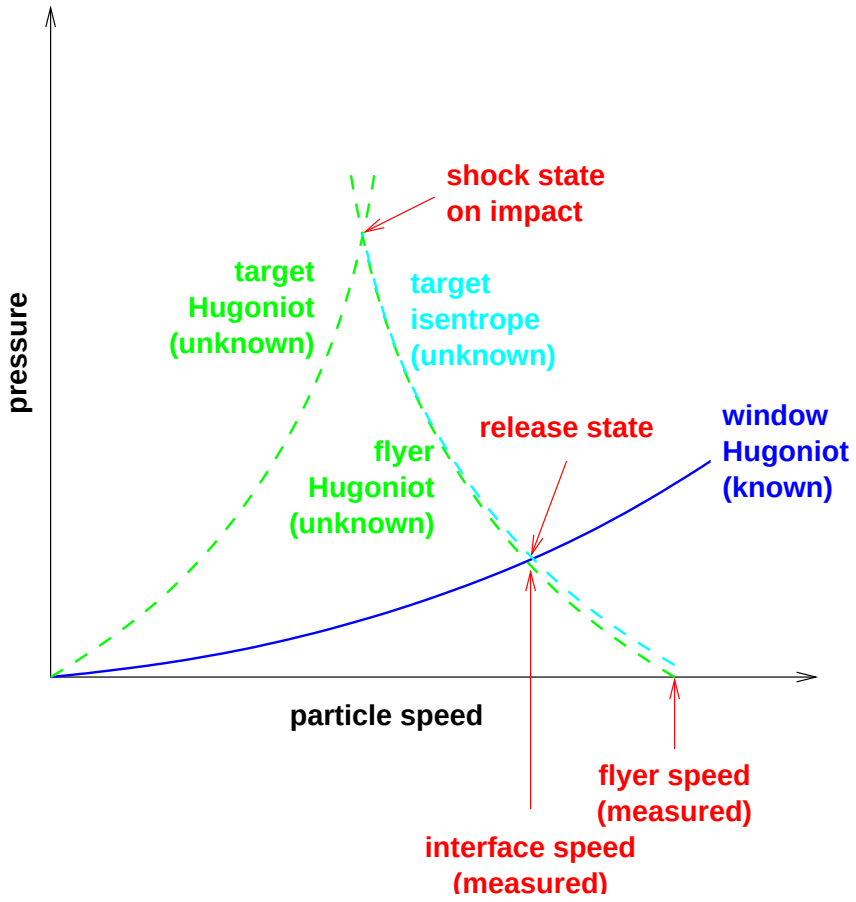

Figure 17: Schematic of construction used to deduce Hugoniot point from window release data with the flyer and target of the same material.

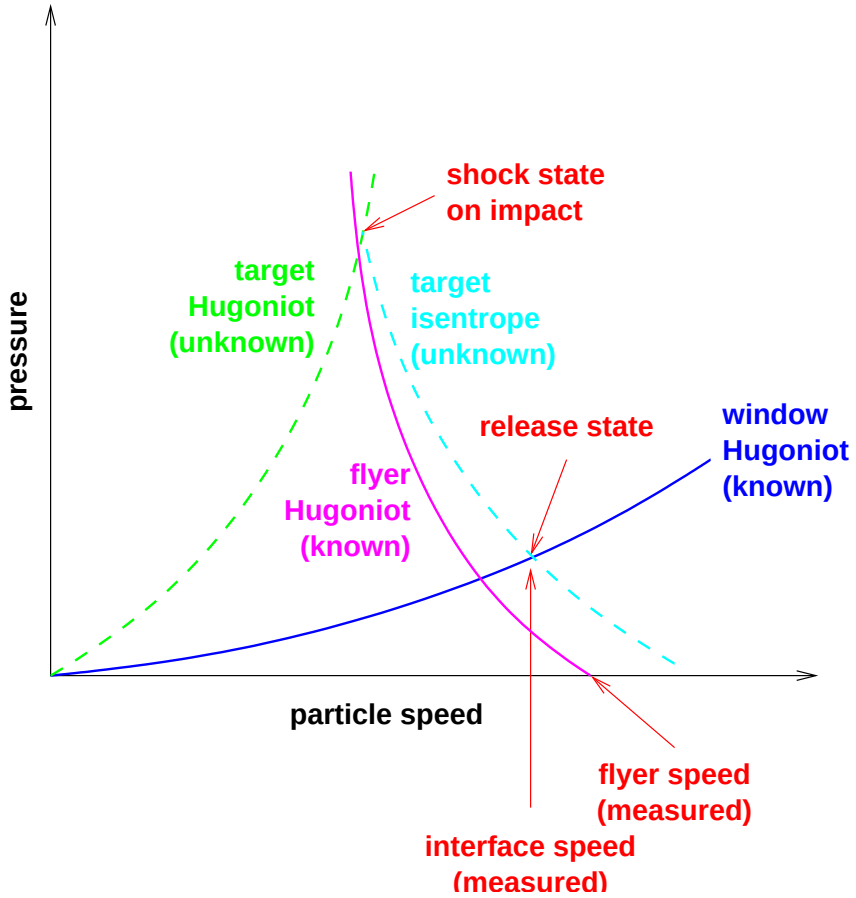

Figure 18: Schematic of construction used to deduce Hugoniot point from window release data with a flyer of known material.

speed at impact.

Reference Hugoniots were calculated from published EOS [10]. The Rankine-Hugoniot equations were solved numerically [11].

The PMMA window was not a good impedance match to NiTi, so the duration of the peak interface speed did not give a direct measurement of the sound speed on the Hugoniot. However, the consistency of an equation of state with the observed duration could be tested.

5.2 Shock Hugoniot

Structures in the velocity history were seen where a simple EOS would give a constant state, e.g. after the initial deceleration on impact with the window, and in the region of peak velocity at the surface of the sample. This was not seen for the impact of copper flyers, so it seems likely to be related to the constitutive behaviour of NiTi. The structure made it more difficult to choose a single velocity, and thus contributed to the uncertainties in EOS points deduced from the data. There is scope for further analysis assuming forms for the constitutive behaviour.

As with any VISAR measurement, the velocity inferred after a jump (as opposed to the continuous change seen in flyer acceleration) is uncertain to an integer multiple of the fringe constant. Ideally, a very large number of measurements could be made to cover impact speeds separated by intervals much smaller than the fringe constant. The other standard technique is to use more than one VISAR, with fringe constants whose common multiple is as large as possible within the constraints of the uncertainty in velocity. In these experiments, the VISARs did not provide redundant data of adequate quality, partly because the fringe constant of the line VISAR was quite close to double that of the point VISAR. In practice, the number of fringe jumps in a velocity discontinuity had to be assumed, based on approximate estimates of the EOS – this is also a standard technique in VISAR analysis. However, the fringe constant of the line VISAR was large enough that a rough progression could be obtained of fringe jumps with flyer speed, so the absolute velocity could be determined with reasonable confidence. On the other hand, the larger fringe constant (and low fringe contrast from the rough surface of the sample) meant that velocities measured from the line VISAR had a greater uncertainty on the scale of a fraction of a fringe than did velocities from the point VISAR; this translates as a greater uncertainty in Hugoniot points deduced from the line VISAR.

Data from the impact of copper flyers on PMMA windows were consistent with the published EOS, suggesting that flyers were not significantly heated by the laser drive and that all sources of uncertainty were taken into account [12].

Hugoniot points were successfully obtained for both alloys. Points from window impact explored pressure $\sim$1 GPa or less, because of the low shock impedance of the PMMA. The window impact experiments with a copper flyer explored pressures $\sim$10 GPa. States deduced by window release and window impact were consistent. The EOS of the 6B alloy seemed to be consistently softer than that of 5B. To the accuracy of these initial experiments, the *ab initio* EOS was consistent with the data for alloy 5B. (Figs 19 to 21.)

5.3 Compressive strength

In some of the velocity records, there was a precursor ahead of the main shock wave. This data can be used to infer elastic and plastic properties (unless confused with phase changes). In the regimes explored by these experiments, the strength can be treated as a correction to the EOS. A larger set of precursor data is desirable before drawing strong conclusions about the strength, so for the time being we summarise only the characteristics of the precursors observed (Table 7). Where a shot is listed but no precursor is given, a suitable experimental record was obtained but no precursor could be distinguished. In some of these experiments, the noise on the velocity record was significant. The precursor has a lower amplitude than the shock wave, so in some cases it could simply be obscured by noise. Uncertainties in precursor characteristics were not estimated. The precursors exhibited some structure, and more data should be obtained to find the best way to describe their shape.

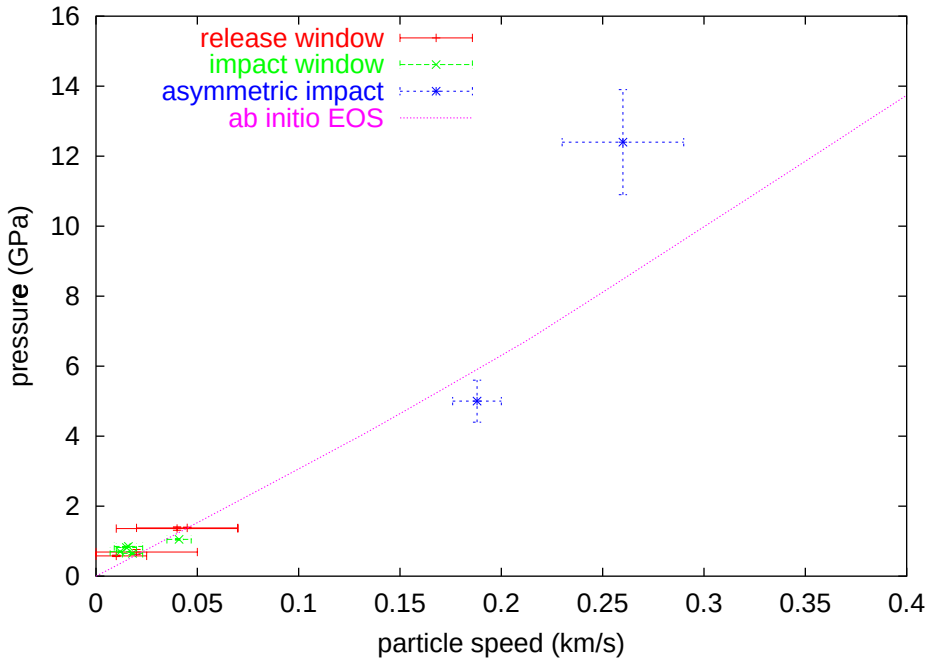

Figure 19: Hugoniot points deduced for alloy 5B.

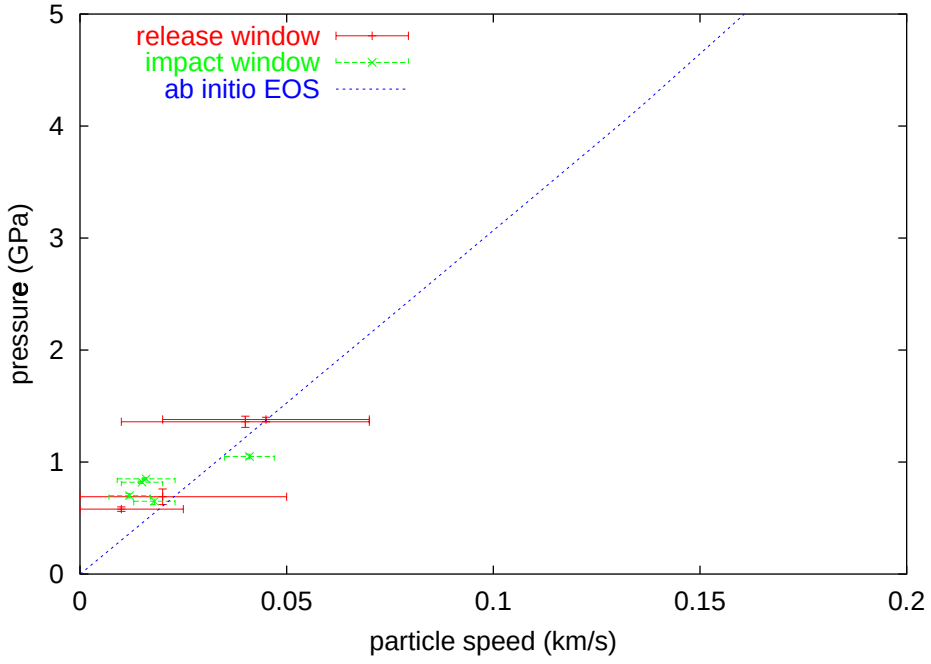

Figure 20: Hugoniot points deduced for alloy 5B – detail at low pressures.

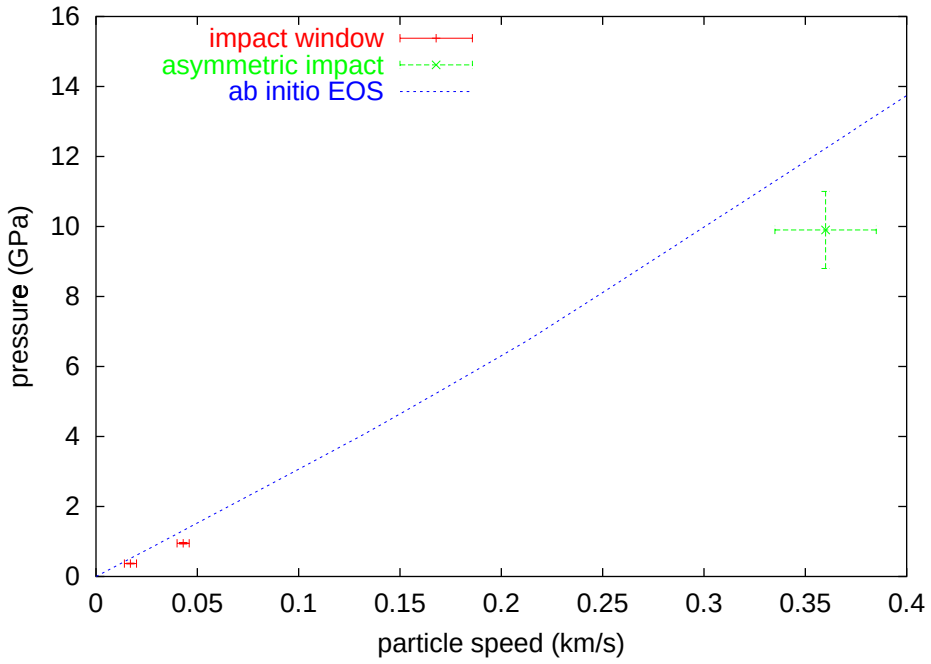

Figure 21: Hugoniot points deduced for alloy 6B.

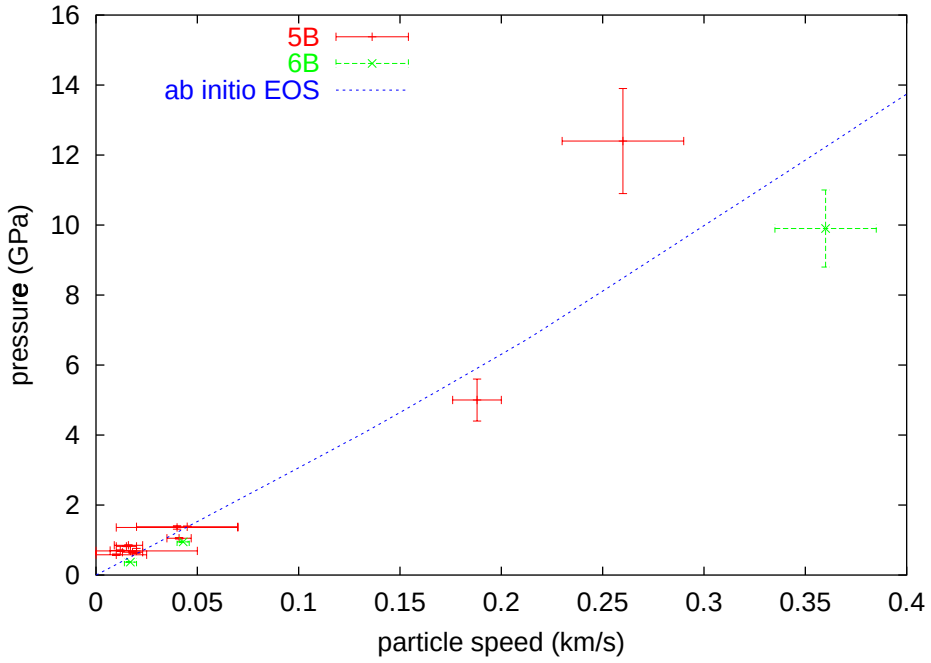

Figure 22: Hugoniot points for alloys 5B (52.5 atomic % Ni) and 6B (55.6 atomic % Ni), compared with the *ab initio* equation of state.

Table 7: Summary of the characteristics of precursor waves.

shot	**particle speed** (m/s)	**rise-time** (ns)	**delay before shock** (ns)	**comments**
14123	30	3	24	
14124	75	1	17	
14125	20	7	25	
14141	70	10	45	rise may be below time resolution
14142	-			
14143	-			
14144	-			
14146	-			
14147	-			
14149	-			
14150	-			
14151	-			

Table 8: Spall strength.

alloy	**spall strength** (GPa)
5B	1.8 ± 0.2
6B	2.4 ± 0.2

5.4 Spall strength

The observed velocity pull-back Δu was averaged for each alloy, and a single spall strength σ deduced from the EOS using the relation

$$\sigma = \frac{1}{2}\rho_0 c_0 \Delta u, \tag{1}$$

where ρ_0 and c_0 are the mass density and sound speed at STP [13]. The 6B alloy seemed to have a higher spall strength. (Table 8.)

6 Conclusions

Experimental Hugoniot points were obtained for NiTi alloys with 52.5 and 55.6 atomic % Ni. The points were all with respect to the Hugoniot of copper or PMMA – shock transit times were not measured accurately enough to be useful for EOS.

The Hugoniot points for the alloy with 52.5% Ni were consistent with the *ab initio* EOS for 50% Ni in the CsCl structure. The alloy with 55.6% Ni was systematically softer.

The characteristics of precursor waves were recorded for future analysis when more data have been obtained.

The spall strength of each alloy was estimated from the velocity pull-back in experiments where the sample released into vacuum.

Several improvements could be made in future experiments. It is important to have a more reflective finish for any surface to be viewed through a window. This is probably preferable to adding an anti-reflection coating to the window, as the layers of different refractive index would affect the Doppler shift after impact. A reasonable compromise would be to coat only the side of the window facing toward the VISAR. It would be easier to determine the Hugoniot over a range of pressures from window impact experiments if a range of different windows were available to cover a range of different shock impedances. The technique of release

into vacuum following impact by a flyer of known properties seems valuable. Strength can be determined from wave profiles following symmetric or anti-symmetric impacts. In order to measure the shock speed, we would need to improve the accuracy or metrology of alignment of fiducial windows, and to run the diagnostics with a smaller time resolution (and hence adequate reproducibility or accuracy in calculating timing and assembling targets). It may be preferable to use wedge-shaped or stepped samples, or to mount the sample on a base-plate of known opaque material.

Acknowledgements

Dan Thoma and Allan Hauer provided funding from their LDRD-ER on the dynamics of martensitic phase changes. We would like to thank the TRIDENT staff including Randy Johnson, Tom Hurry, Tom Ortiz, Fred Archuleta, Nathan Okamoto, and Ray Gonzales for their hard work on the experiments. Dennis Paisley provided experimental advice and help with the analysis and interpretation of VISAR records. George Kyrala reviewed and corrected the draft of this report.

References

[1] D.C. Swift and D.L. Paisley, *Laser-Induced Shock Experiments on NiTi Alloys*, LA-UR-00-5871 (2000).

[2] D.C. Swift and D.L. Paisley, *Analysis of Laser-Induced Shock Experiments on NiTi Alloys*, LA-UR-01-853 (2001).

[3] D.C. Swift and G.J. Ackland, *First-principles predictions of the mechanical properties of nickel - titanium alloy*, LA-UR-00-5049 (2000).

[4] R. Hackenberg and K. Chen, analysis of microstructure of recovered NiTi samples, unpublished.

[5] D.C. Swift, *An ab initio Grüneisen equation of state for nickel – titanium alloy*, LA-UR-02-0903 (2002).

[6] D.L. Paisley, D.C. Swift, R.P. Johnson, J.C. Lashley and J.G. Niemczura, *Flyer plates launched with long laser pulses*, LA-UR-01-5814 (2001).

[7] D.C. Swift, *Laser-launched flyers from PMMA substrates*, LA-UR-02-0905 (2002).

[8] D.C. Swift, *Derivation of VISAR fringe constants*, LA-UR-02-0904 (2002).

[9] Melles Griot catalog, Melles Griot Corp (2001).

[10] D.J. Steinberg, *Equation of state and strength properties of selected materials*, Lawrence Livermore National Laboratory report UCRL-MA-106439 change 1 (1996).

[11] 'ELECTRA' software and manual, Wessex Scientific and Technical Services Ltd (2000).

[12] D.C. Swift, *Accuracy of laser-launched flyers for measuring equations of state*, LA-UR in preparation (2002).

[13] A V Bushman, G I Kanel', A L Ni and V E Fortov, "Intense Dynamic Loading of Condensed Matter", Taylor and Francis (1993).

[14] O. Schulte and W. B. Holzapfel, Phys Rev B **48**, 767 (1993).